



EZH2 is associated with cartilage degeneration in osteoarthritis by promoting SDC1 expression *via* histone methylation of the microRNA-138 promoter

Jian Wang¹ · Xiang Wang² · Xu Ding¹ · Tao Huang¹ · Dengxin Song¹ · Hairong Tao²

Received: 10 August 2020 / Revised: 3 December 2020 / Accepted: 16 December 2020 / Published online: 10 March 2021
© The Author(s), under exclusive licence to United States and Canadian Academy of Pathology 2021

Abstract

Cartilage degeneration has been reported to deteriorate osteoarthritis (OA), a prevalent joint disease caused by intrinsic and epigenetic factors. This study aimed to examine the molecular mechanism of enhancer of zeste 2 polycomb repressive complex 2 subunit (EZH2)/microRNA-138 (miR-138)/syndecan 1 (SDC1) and its epigenetic regulation in cartilage degeneration in OA. An OA cell model was induced by stimulating chondrocytes with interleukin (IL)-1 β at a final concentration of 10 ng/mL, followed by alterations in EZH2 and miR-138 expression. Afterwards, cell apoptosis was analyzed using flow cytometry. The expression patterns of cartilage catabolism-related factors (MMP-13, ADAMTS-4, and ADAMTS-5) were determined using RT-qPCR and western blot analyses. The EZH2 and H3K27me3 enrichment at the miR-138 promoter region were determined using ChIP-qPCR. Finally, an OA mouse model was constructed to verify the function of EZH2 *in vivo*. EZH2 was expressed at high levels in OA models. EZH2 depletion ameliorated OA, as evidenced by reduced cell apoptosis in IL-1 β -treated chondrocytes and decreased levels of cartilage catabolism-related factors. Moreover, EZH2 promoted histone methylation at the miR-138 promoter to suppress miR-138 expression, thereby upregulating the expression of SDC1, a target gene of miR-138. Changes in this pathway increased the expression of cartilage catabolism-related factors *in vitro* while promoting cartilage degeneration *in vivo*. Our data provided evidence that EZH2 inhibits miR-138 expression by promoting the histone methylation of its promoter, which induces cartilage degeneration in OA models by upregulating SDC1 expression, suggesting a novel mechanistic strategy for OA treatment.

Introduction

Osteoarthritis (OA) is characterized by the loss of joint function and increasing pain and progresses to a critical threat to human health. Moreover, the slow progression of the disease causes sustained and chronic pain in patients. Thus, a better understanding of the pathological process of OA is imperative for the development of effective therapies [1]. Degeneration of the articular cartilage is a

typical symptom of OA and primarily occurs due to chondrocyte apoptosis [2, 3]. Additionally, cartilage degeneration is also implicated in the development of OA, which further induces the production of pro-inflammatory cytokines, including interleukin (IL)-1 β , thus invoking an inflammatory response [4]. Numerous studies have attempted to elucidate the underlying mechanism mediating cartilage degeneration. For example, Wang et al. have reported the involvement of DNA methylation in chondrocyte apoptosis in knee OA by modifying genetic expression [5]. However, the detailed mechanism by which DNA methylation modulates OA remains to be elucidated.

Notably, enhancer of zeste 2 polycomb repressive complex 2 subunit (EZH2), one of the polycomb repressive complex 2 catalytic subunits, potentially directs histone methylation and promotes H3 lysine-27 trimethylation (H3K27me3) [6]. Moreover, EZH2 has also been reported to affect OA development by regulating the Wnt/ β -catenin

✉ Hairong Tao
taohair@163.com

¹ Department of Orthopedics, Zhongshan Hospital Wusong Branch, Fudan University, 200940 Shanghai, PR China

² Shanghai Key Laboratory of Orthopaedic Implants, Department of Orthopaedic Surgery, Shanghai Ninth People's Hospital, Shanghai Jiao Tong University School of Medicine, 200011 Shanghai, PR China

pathway [7]. Accordingly, EZH2 was shown to be involved in microRNA (miR)-128a methylation, which further regulates the degree of OA [8]. Based on these findings, we anticipated the existence of other potential miRNAs that possibly interact with EZH2. Intriguingly, one miRNA was miR-138, which modulates cell survival and regulates chondrocytes in OA through the Wnt/ β -catenin pathway [9]. Coincidentally, after reviewing the literature, we found that EZH2 interacts with miR-138 and regulates miR-138 expression *via* EZH2-induced methylation in multiple myeloma [10]. However, the effect of this interaction on cartilage degeneration or OA remains unknown. On the other hand, syndecan 1 (SDC1) and WIN55 function in human OA articular chondrocytes [11]. Moreover, previous studies have reported a regulatory relationship between SDC1 and different miRNAs, such as hsa-miR-19b and hsa-miR-19a [12]. However, a comprehensive understanding of the correlation between SDC1 and miR-138 in OA remained to be elucidated.

Accordingly, the present study attempted to provide evidence that EZH2 is essential for cartilage degeneration in OA and affects the progression of OA by mediating histone methylation. Moreover, OA cell models and OA cartilage tissues were employed to explore the regulatory mechanism of EZH2 in the process of OA. By determining the interactions of EZH2/miR-138/SDC1, we speculated that epigenetic modifications were involved in the development of OA, hence providing a contemporary basis for the development of a potential therapeutic target for OA.

Materials and methods

Bioinformatics analysis

The OA-related microarray GSE82107 dataset comprising ten OA synovioocyte samples and seven normal synovioocyte samples was retrieved from the Gene Expression Omnibus database (<https://www.ncbi.nlm.nih.gov/geo/>). Subsequently, using a \log_2 of fold change > 2 and p value < 0.05 as the threshold value, the limma microarray package was employed to screen the differentially expressed genes (DEGs) enriched in OA. Then, a protein–protein interaction (PPI) analysis of DEGs with a confidence coefficient of 0.4 was conducted using the STRING online website. The results of the PPI analysis were subsequently visualized with the Cytoscape software to screen DEGs with a degree value ≥ 2 . Lastly, the upstream regulatory miRNAs of the DEGs were predicted using the miRanda (<http://www.microrna.org/microrna/home.do>) and Starbase databases (<http://starbase.sysu.edu.cn/>). The predicted miRNAs were finally intersected.

Cell culture and identification

Extraction and culture of human chondrocytes

OA articular cartilage tissues were acquired from 25 patients with OA (10 males, 15 females; aged 31–63 years, with a mean age of 48.68 ± 9.57 years) (grade III–IV) who underwent total knee arthroplasty at Shanghai Ninth People's Hospital, Shanghai Jiao Tong University School of Medicine. In addition, another 25 normal articular cartilage tissues were collected from patients (11 males, 14 females; aged 37–65 years, with a mean age of 47.72 ± 7.83 years old) who underwent amputation surgery or corrective surgery. Moreover, cartilage sections were harvested from human samples (healthy and OA articular cartilage tissues). Then, normal and OA cartilage tissues were digested with 0.25% trypsin for 30 min and then cultured in Dulbecco's Modified Eagle's Medium with Ham's F-12 medium (DMEM/F12) containing antibiotics and 2 mg/mL collagen II (Col II) at 37 °C for 6 h. Thereafter, cells were suspended, seeded in tissue culture flasks, and cultured with DMEM/F12 supplemented with 10% fetal bovine serum and 1% penicillin–streptomycin at 37 °C in the presence of 5% CO₂.

The isolated chondrocytes were trypsinized and cultured in a 24-well plate coated with polylysine at a density of 2×10^4 cells/well for 24 h. The cells were then fixed with 95% ethyl alcohol for 20 min and stained with 1% toluidine blue in ethanol for 20 min. Subsequently, the cells were mounted, observed, and photographed using an inverted fluorescence microscope.

Cell slides were prepared used similar procedures as described above, and identified using Col II immunofluorescence staining. Briefly, cells were fixed with 4% paraformaldehyde for 20 min, permeabilized with 0.2% Triton X-100 for 10 min, and incubated with phosphate-buffered saline containing 1% bovine serum albumin for 15 min. Subsequently, the cells were probed with a rabbit polyclonal antibody against Col II (1:5000; ab34712; Abcam Inc., Cambridge, UK) overnight at 4 °C and then re-probed with a DyLight 488-conjugated goat anti-rabbit fluorescent secondary antibody (A23220; Abbkine, CA, USA) for 1 h. Finally, the cells were stained with 4',6-diamidino-2-phenylindole for 30 min, mounted, observed, and photographed.

Construction of OA cell models

Normal human chondrocytes were treated with IL-1 β (Sigma-Aldrich; Merck KGaA; St. Louis, MO, USA) at a final concentration of 10 ng/mL [13, 14] and then incubated with 5% CO₂ in a 37 °C incubator for 24 h. Cells that did not receive a treatment were selected as controls. Then, the chondrocytes were observed under the microscope and we

observed cytoplasmic shrinkage and vacuoles in chondrocytes, indicating the successful establishment of the model, with a success rate of 100%.

Cell grouping and transfection

Following OA model construction, cells were treated with a small interfering RNA sequence targeting EZH2 (si-EZH2), miR-138 mimic plasmids, interleukin (IL)-1 β , 3-deazaneplanocin A (1 μ M; an inhibitor of EZH2) [15], or their relevant negative controls (NC), alone or in combination. The aforementioned overexpression vector pcDNA3.1 was developed by Invitrogen Inc., (Carlsbad, CA, USA) and the remaining plasmids were designed and established by Shanghai GenePharma Co., Ltd (Shanghai, China). 3-Deazaneplanocin A was purchased from MedChemExpress (MCE, HY-10442, USA). Cells at 30–50% confluence were transfected with the aforementioned plasmids. After 12 h, the culture medium was replaced upon achieving more than 95% of viable cells. Then, at 72 h post culture, the transfected cells were collected and a Western blot analysis was performed to assess the transfection efficiency of overexpression or knockdown plasmids. The sequences of miR-138, si-NC and si-EZH2 were as follows: miR-138 mimic (5'-AGCUGGUGUUGUGAAUCAGGCCG-3') [16], si-NC (sense: 5'-UUCUCCGAACGUGU-CACGUdTdT-3'; antisense: 5'-ACGUGACACGUUCGGAGAAdTdT-3'), and si-EZH2 (sense: 5'-GACACCCG-GUGGGACUCAGAAG-3'; antisense: 5'-CUUCUGA-GUCCACCCGGUGUC-3') [17]. The subsequent transfection was conducted using the Lipofectamine 2000 reagent (Invitrogen) according to the manufacturer's protocol. The transfection efficiency was 90–100%. After 72 h of culture, the stably transformed cells were collected and used in subsequent experiments.

RNA isolation and quantification

Total RNA was extracted using the RNeasy Mini Kit (Qiagen, Valencia, CA, USA). For mRNA detection, the extracted RNA was reverse transcribed into complementary DNAs (cDNAs) using reverse transcription kits (RR047A; Takara, Tokyo, Japan). For miRNA detection, the extracted RNA was reverse transcribed into cDNAs using the miRNA First Strand cDNA Synthesis (Tailing Reaction) kit (B532451-0020; Sangon, Shanghai, China). Samples were amplified using the SYBR[®] Premix Ex Taq[™] II (Perfect Real Time) kits (DRR081; Takara). Reverse transcription-quantitative polymerase chain reaction (RT-qPCR) was subsequently conducted using an ABI 7500 instrument (Applied Biosystems, Foster City, CA, USA). Three replicate wells were established for each condition. The miRNA universal negative primers and U6 (human and mouse)

Table 1 Primer sequences for RT-qPCR.

Target	Primer sequences
EZH2 (H)	F: 5'-AATCAGAGTACATGCGACTGAGA-3' R: 5'-GCTGTATCCTTCGCTGTTTCC-3'
miR-138 (H)	F: 5'-AGCTGGTGTGTGAATCAGGCCG-3'
SDC1 (H)	F: 5'-CCACCATGAGACCTCAACCC-3' R: 5'-GCCACTACAGCCGTATTCTCC-3'
MMP-13 (H)	F: 5'-ACTGAGAGGCTCCGAGAAATG-3' R: 5'-GAACCCCGCATCTTGGCTT-3'
ADAMTS-4 (H)	F: 5'-GAGGAGGAGATCGTGTTCCTCA-3' R: 5'-CCAGCTCTAGTAGCAGCGTC-3'
ADAMTS-5 (H)	F: 5'-GAACATCGACCAACTCTACTCCG-3' R: 5'-CAATGCCACCGAACCATCT-3'
β -actin (H)	F: 5'-AACAGTCCGCTAGAAGCAC-3' R: 5'-CGTTGACATCCGTAAGACC-3'
EZH2 (M)	F: 5'-AGTGACTTGGATTTCCAGCAC-3' R: 5'-AATTCTGTTGTAAGGGCGACC-3'
miR-138 (M)	F: 5'-GCCGATAAGTGTGTGGTCGA-3'
SDC1 (M)	F: 5'-AGCAACACCGAGACTGCTTTT-3' R: 5'-GTGCGGATGAGATGTGACAG-3'
MMP-13 (M)	F: 5'-CTTCTTCTGTTGAGCTGGACTC-3' R: 5'-CTGTGGAGGTCCTGTAGACT-3'
ADAMTS-4 (M)	F: 5'-ATGGCCTCAATCCATCCAG-3' R: 5'-AAGCAGGGTTGGAATCTTTGC-3'
ADAMTS-5 (M)	F: 5'-GGAGCGAGCCATTTACAAC-3' R: 5'-CGTAGACAAGGTAGCCACTTT-3'
β -actin (M)	F: 5'-GGTGAGGTCCTTGCCTACTT-3' R: 5'-CCTCTATGCCAACACAGTGC-3'
ChIP	F: 5'-CTGCCACTTGTTCGAACCGA-3' R: 5'-GCACGGCCCAGCACACAAAGA-3'

RT-qPCR reverse transcription-quantitative polymerase chain reaction, *EZH2 (H)* enhancer of zeste 2 polycomb repressive complex 2 subunit (human), *EZH2 (M)* enhancer of zeste 2 polycomb repressive complex 2 subunit (mouse), *miR-138* microRNA-138, *SDC1* syndecan 1, *MMP-13* matrix metalloproteinase 13, *ADAMTS-4* ADAM metalloproteinase with thrombospondin type 1 motif 4, *ChIP* chromatin immunoprecipitation, *F* forward, *R* reverse.

upstream primers were provided by the miRNA First Strand cDNA Synthesis (Tailing Reaction) kit. Other primers were synthesized by Sangon Biotech Co., Ltd. (Shanghai, China) (Table 1). After normalization to U6 as the loading control for miR-138 and to glyceraldehyde-3-phosphate dehydrogenase as the loading control for the remaining genes, relative expression was analyzed using the $2^{-\Delta\Delta C_t}$ method.

Western blot analysis

Total protein was extracted from tissues or cells using radioimmunoprecipitation assay lysis buffer supplemented with phenylmethylsulfonyl fluoride. The extracted proteins were then separated using sodium dodecyl sulfate-

polyacrylamide gel electrophoresis and transferred onto a polyvinylidene fluoride (PVDF) membrane. The PVDF membrane was then incubated at 4 °C overnight with the diluted primary rabbit antibodies (Cell Signaling Technology, Danvers, MA, USA) against EZH2 (1:1000; 4905S) and SDC1 (1:1000; 12922S), while a rabbit antibody against β -actin (1:1000; 4970S) was used as the internal reference. On the next day, after washes with Tris-buffered saline containing Tween-20, the membrane was incubated with horseradish peroxidase-conjugated goat anti-rabbit immunoglobulin G (IgG) (1:2000; ab97051; Abcam) for 1 h and developed with enhanced chemiluminescence reagent (BB-3501; Amersham Biosciences, Piscataway, NJ, USA). The band intensities were photographed using the Bio-Rad Image analysis system (Bio-Rad, Hercules, CA, USA) and analyzed using Quantity One v4.6.2 software. The relative protein level was calculated as the ratio of the gray value of the target band to the β -actin band. Each experiment was repeated 3 times to obtain the mean value.

Dual-luciferase reporter gene assay

The pmirGLO luciferase reporter plasmids containing wild type (WT) and mutant (MUT) SDC1 were designed by GenePharma (Shanghai, China). Then, the WT-SDC1-3' untranslated region (3'UTR) and MUT-SDC1-3'UTR were co-transfected with the NC mimic and miR-138 mimic respectively into the OA cell models. Cells were collected 48 h after transfection and then lysed. The subsequent procedures were performed using a luciferase assay kit (K801-200; BioVision, Milpitas, CA, USA) and the analysis system (Promega Corporation, Madison, WI, USA). The relative luciferase (RLU) activity was calculated as the ratio of the RLU activity of firefly luciferase/RLU activity of Renilla luciferase. Each experiment was repeated 3 times to obtain the mean value.

Chromatin immunoprecipitation (ChIP)

The ChIP assay was performed using the EZ-Magna ChIP A/G kits (17-371; Millipore, Billerica, MA, USA). Briefly, the cells were sonicated and centrifuged at $12000 \times g$ for 10 min at 4 °C to remove the insoluble precipitate. Then, the cells were incubated with Protein G Agarose at 4 °C for 1 h and centrifuged at $5000 \times g$ for 1 h, followed by the removal of the supernatant. Ten microliters of the supernatant (1%) were then removed and used as the input, while the remaining supernatant was divided into three aliquots and incubated with antibodies against EZH2 (1:25; 4905S; Cell Signaling Technology), H3K27me3 (1:50; 9733S; Cell Signaling Technology), and NC rabbit anti-human IgG (1:25; ab2410; Abcam) at 4 °C overnight. The protein-DNA complex was precipitated by an incubation with Protein G

Agarose at 4 °C for 1 h, followed by the removal of the crosslinks. DNA fragments were purified, collected, and then used as an amplification template for RT-qPCR. Primer sequences are shown in Table 1.

Flow cytometry

Cells were collected 48 h after transfection. Then, cell apoptosis was analyzed using the Annexin V-fluorescein isothiocyanate (FITC) Apoptosis Assay Kits (BD Biosciences, San Jose, CA, USA). After Annexin V-FITC-propidium iodide double staining, cells were analyzed using a flow cytometer (FACSCalibur; BD Biosciences).

Experimental OA mouse models and lentivirus injection

Seventy C57BL/6J WT mice (aged 8 weeks; weighing 18–22 g, with a mean calculated weight of 19.55 ± 1.02 g) were purchased from the Laboratory Animal Center of Shanghai Ninth People's Hospital, Shanghai Jiao Tong University School of Medicine. All mice were housed on a 12 h light/dark cycle with free access to water and food. Then, the OA model was established in 60 mice via an operation. Briefly, the right medial collateral ligaments and anterior cruciate ligaments of OA model mice were removed, followed by transection of the medial meniscus in the right knee. Meanwhile, the remaining ten mice were subjected to a sham operation in which only the skin of the mouse right knee joint was incised. Before the surgical procedure, all mice were anesthetized with an intraperitoneal injection of pentobarbital sodium at a dose of 40 mg/kg [18], and the mice were euthanized 5 weeks after knee surgery to collect the knee joint specimens. The success rate of OA modeling was 83.3%.

The recombinant lentivirus and agomir were designed by HanBio (Shanghai, China). Then, mice were divided into the sham group (mice that received the sham operation), the OA group (mice that underwent OA modeling), the OA + Lv-oe-NC + agomir-NC group (mice injected with lentivirus-mediated nonsense control and miRNA overexpression sequence), the OA + Lv-oe-EZH2 + agomir-NC group (mice injected with EZH2 overexpression lentivirus and nonsense miRNA sequence), and the OA + Lv-oe-EZH2 + miR-138 agomir group (mice injected with EZH2 overexpression lentivirus and miR-138 overexpression sequence), with ten mice in each group. The lentivirus vector was injected at a volume of 10 μ L (4×10^8 TU/mL), while agomir-NC and miR-138 agomir were injected at a dose of 250 μ M [19]. On days 7 and 14 after model establishment, OA mice were injected with the corresponding lentiviruses, miR-138 agomir, or agomir NC, twice per injection [19]. At 5 weeks after model

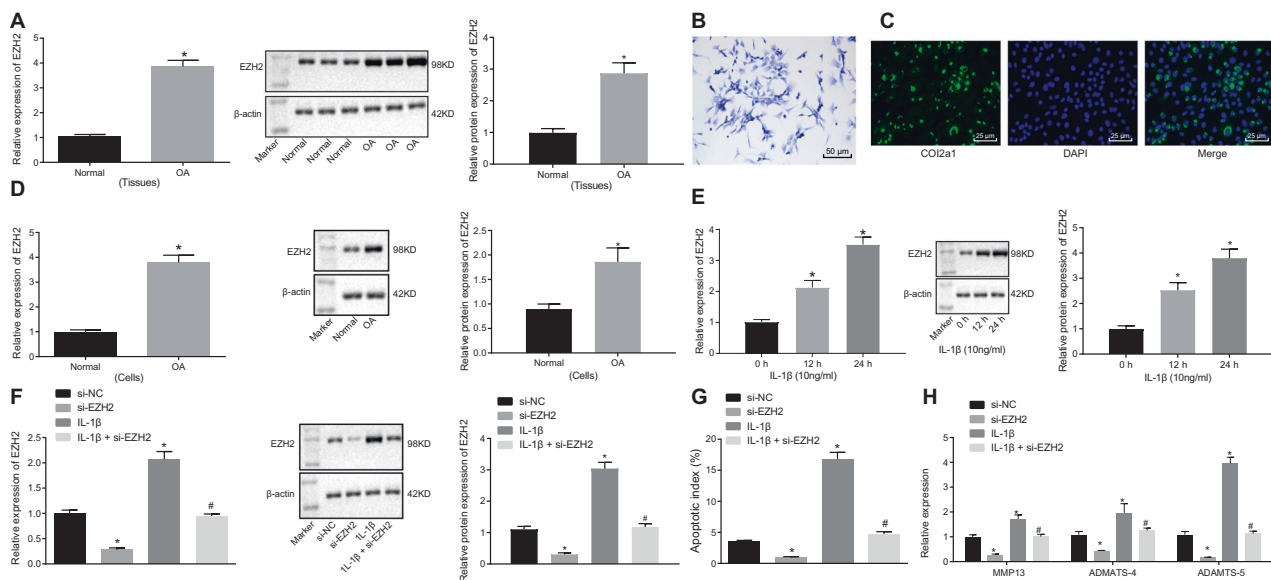


Fig. 1 The expression of EZH2 in OA and its effect on OA. **A** EZH2 expression patterns in OA and healthy articular cartilage tissues detected using RT-qPCR and western blotting. $*p < 0.05$ compared with healthy articular cartilage tissues ($n = 25$). Representative Western blot images are presented. **B** Toluidine blue staining ($\times 200$). **C** Col II immunofluorescence staining ($\times 400$), from the left to the right, positive staining, spontaneous fluorescence and a merged image are shown. **D** EZH2 expression patterns in OA and normal chondrocytes after 48 h of culture, as measured using RT-qPCR and western blotting. $*p < 0.05$ compared with normal chondrocytes.

E EZH2 expression detected at 0, 12, and 24 h after IL-1 β treatment using RT-qPCR and western blotting. **F** EZH2 expression in normal chondrocytes receiving various treatments in the presence/absence of IL-1 β (10 ng/mL), as analyzed using RT-qPCR and western blotting. **G** Cell apoptosis detected by flow cytometry. **H** Expression of biomarkers of cartilage catabolism (MMP-13, ADAMTS-4, and ADAMTS-5) determined using RT-qPCR. $n = 3$. In (**E**, **F**), $*p < 0.05$ compared with cells transfected with si-NC; $\#p < 0.05$ compared with cells treated with IL-1 β .

establishment, mice were euthanized by carbon dioxide inhalation, and the articular cartilage tissue from the right knee was frozen in liquid nitrogen or embedded in paraffin.

Safranin O staining

Paraffin sections were stained with the fast green solution for 5 min, washed with a 1% acetic acid solution for 15 s, and then stained with a 0.1% safranin O solution for 5 min. Next, the sections were dehydrated twice with 95% ethyl alcohol, absolute ethyl alcohol, and xylene, respectively (2 min each). Finally, the sections were photographed with a Zeiss AxioCam digital camera, and the pathological grade of OA mice was evaluated using the Osteoarthritis Research Society International (OARSI) scoring system.

Statistical analysis

All statistical analyses of the data were performed with SPSS 22.0 software (IBM Corp., Armonk, NY, USA), and the results are presented as the means \pm standard deviations. Differences between the two groups were determined using an unpaired t test, while one-way analysis of variance was performed to determine statistically significant differences among multiple groups, followed by

Tukey's post hoc test. The correlations between the expression of various cytokines in OA models were analyzed by calculating Pearson's correlation coefficients. In all statistical analyses, $p < 0.05$ represents statistical significance.

Results

EZH2 was upregulated in OA models, and EZH2 knockdown suppressed OA progression

RT-qPCR and western blot analyses were employed to determine the expression patterns of EZH2 in OA and healthy articular cartilage tissues (Fig. 1A). EZH2 was expressed at much higher levels in OA articular cartilage tissues than in healthy articular cartilage tissues ($p < 0.05$). Then, OA chondrocytes and normal chondrocytes were obtained from OA and healthy articular cartilage tissues, respectively, after primary culture. Since proteoglycan and Col II are the main indicators of chondrocyte function, toluidine blue staining (Fig. 1B) and Col II immunofluorescence staining (Fig. 1C) were performed, respectively. Monolayer cells displaying polygonal growth and a bluish-violet cytoplasm or cells in which the cytoplasm and membrane exhibited distinct green fluorescence and a

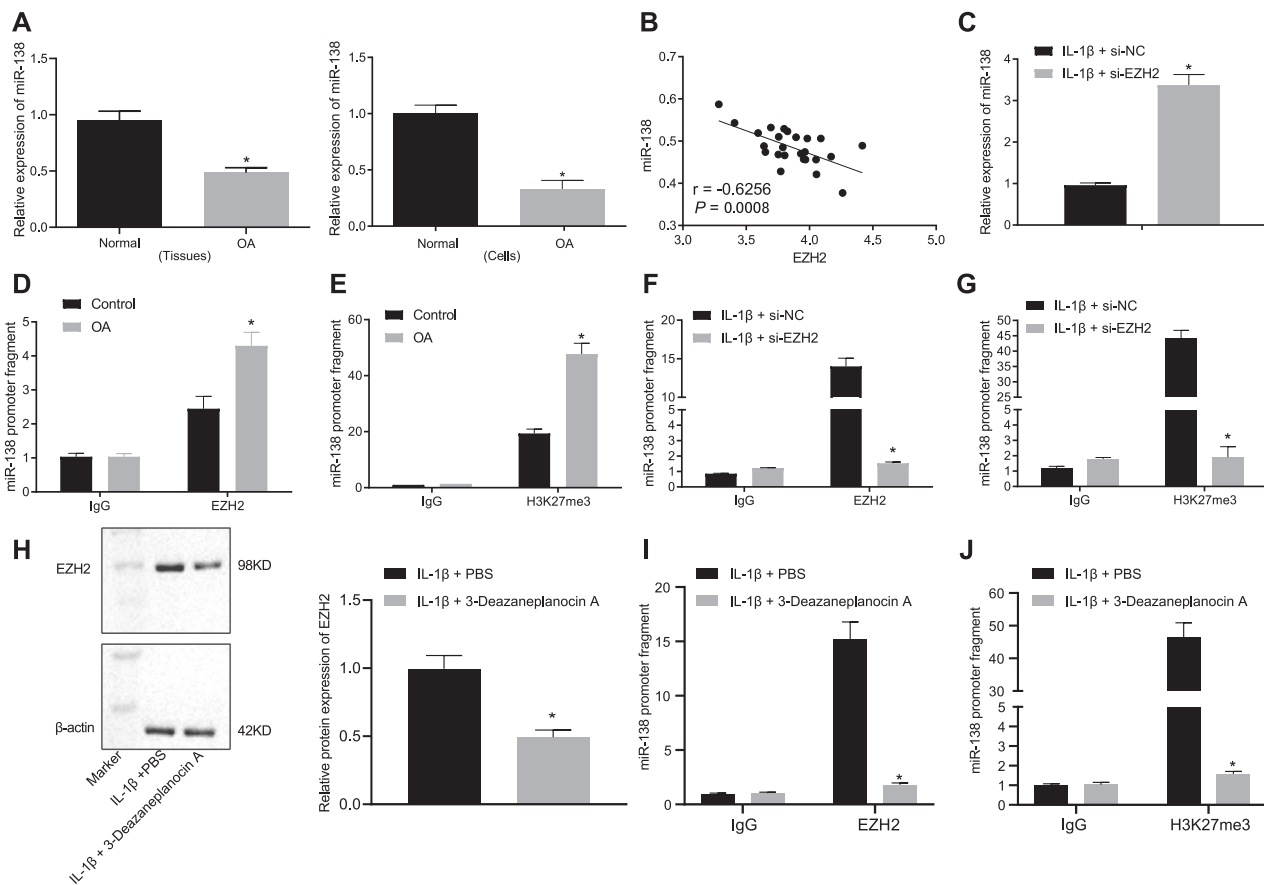


Fig. 2 The regulatory relation between EZH2 and histone methylation at the miR-138 promoter. **A** Expression of miR-138 in OA cartilage tissue and the OA cell model determined using RT-qPCR. $*p < 0.05$ compared with healthy cartilage tissues or normal chondrocytes ($n = 25$). **B** Pearson's correlation coefficients between EZH2 and miR-138 expression in OA cartilage tissues ($n = 25$) determined by calculating Pearson's correlation coefficient. **C** Expression of miR-138 after EZH2 knockdown in the OA cell model, as measured using RT-qPCR. $*p < 0.05$ compared with the OA cell model with si-NC transfection. **D** Content of the miR-138 promoter immunoprecipitated by the EZH2 antibody in OA and normal chondrocytes, as analyzed using ChIP and RT-qPCR. $*p < 0.05$ compared with OA cell models. **E** The quantity of the miR-138 promoter immunoprecipitated by the H3K27me3 antibody in OA and normal chondrocytes, as analyzed using the ChIP-qPCR. $*p < 0.05$ compared with OA cell models. **F** The quantity of the miR-138

promoter immunoprecipitated by the EZH2 antibody after EZH2 knockdown, as detected using ChIP-qPCR. $*p < 0.05$ compared with cells transfected with si-NC. **G** The quantity of the miR-138 promoter immunoprecipitated by the H3K27me3 antibody after EZH2 knockdown. $*p < 0.05$ compared with cells transfected with si-NC. **H** Western blot showing EZH2 levels in OA cells treated with IL-1 β alone or in combination with 3-deazaneplanocin A. $*p < 0.05$ compared with OA cells treated with IL-1 β + PBS. **I** The quantity of the miR-138 promoter immunoprecipitated by the EZH2 antibody in cells treated with IL-1 β alone or in combination with 3-deazaneplanocin A, as detected using ChIP-qPCR. $*p < 0.05$ compared with OA cells treated with IL-1 β + PBS. **J** The quantity of the miR-138 promoter immunoprecipitated by the H3K27me3 antibody in cells treated with IL-1 β alone or in combination with 3-deazaneplanocin A, as detected using ChIP-qPCR. $*p < 0.05$ compared with OA cells treated with IL-1 β + PBS. $n = 3$.

comparatively large, circular or oval, and blue nucleus located in the center of the cells were regarded as chondrocytes. Additionally, our results of RT-qPCR and western blot analyses (Fig. 1D) revealed increased EZH2 expression in OA chondrocytes ($p < 0.05$).

To our knowledge, the pro-inflammatory cytokine IL-1 β represents one of the pathogenic factors leading to OA [20]. The RT-qPCR and Western blot analyses revealed that EZH2 expression in normal chondrocytes was increased by the IL-1 β (10 ng/mL) treatment in a time-dependent manner (Fig. 1E). Then, the OA cell model was constructed after normal chondrocytes were subjected to the IL-1 β (10 ng/mL)

treatment for 24 h. Normal chondrocytes were treated with si-NC, si-EZH2, IL-1 β , or the combination of si-EZH2 and IL-1 β to investigate the effect of EZH2 knockdown on both normal chondrocytes and the OA cell model. Subsequently, the EZH2 expression patterns were determined using RT-qPCR and Western blot analyses (Fig. 1F), and EZH2 expression was significantly decreased in the cells with EZH2 silencing, but a significant increase was observed in the cells treated with IL-1 β compared to the si-NC treatment (all $p < 0.05$). Additionally, EZH2 expression was also distinctly reduced following dual treatment with si-EZH2 and IL-1 β compared to treatment with IL-1 β alone ($p < 0.05$).

Subsequently, flow cytometry was performed to analyze cell apoptosis after the various treatments (Fig. 1G). According to the results, apoptosis was reduced in the cells treated with si-EZH2, but increased following the IL-1 β treatment compared to the si-NC-treated cells (all $p < 0.05$). In contrast to the IL-1 β treatment, apoptosis was markedly decreased after treatment with IL-1 β in cells transfected with si-EZH2 ($p < 0.05$). Finally, biomarkers of cartilage catabolism, including matrix metalloproteinase 13 (MMP-13), a disintegrin and metalloproteinase with thrombospondin motifs 4 (ADAMTS-4), and ADAMTS-5 were detected in cells receiving various treatments using RT-qPCR (Fig. 1H). The expression of MMP-13, ADAMTS-4, and ADAMTS-5 was significantly decreased in cells treated with si-EZH2 (compared with si-NC) and with the combination of IL-1 β and si-EZH2 (compared with treatment with IL-1 β alone). However, the expression of MMP-13, ADAMTS-4, and ADAMTS-5 was significantly increased upon treatment with IL-1 β compared to the si-NC treatment (all $p < 0.05$). Based on these findings, EZH2 expression was upregulated in OA and promoted the progression of OA.

EZH2 inhibited miR-138 expression by promoting histone methylation on the miR-138 promoter

In an attempt to discover the downstream regulatory mechanism underlying the effect EZH2 on cartilage degeneration in OA, we reviewed the relevant literature and found that miR-138 is expressed at low levels in human OA cartilage tissues and that miR-138 overexpression inhibits the progression of OA [21]. Furthermore, EZH2 inhibits miR-138 expression by promoting the methylation of histones at the miR-138 promoter in multiple myeloma [10]. Thus, we anticipated that EZH2 would similarly regulate the expression of miR-138 in OA cell models.

The expression of miR-138 was detected in both OA cartilage tissues and cell models using RT-qPCR to further verify our hypothesis (Fig. 2A). A substantial reduction in miR-138 expression was observed in both OA cartilage tissues and OA cell models compared to the respective controls (all $p < 0.05$). Meanwhile, Pearson's correlation analyses revealed a negative correlation of EZH2 with miR-138 expression in OA cartilage tissues ($n = 25$) (Fig. 2B). Moreover, OA cell models were treated with a siRNA targeting EZH2 and its NC, after which miR-138 expression was measured using RT-qPCR (Fig. 2C). Substantially higher miR-138 expression was observed in cells transfected with si-EZH2 than cells transfected with its NC ($p < 0.05$). Then, the quantity of the miR-138 promoter immunoprecipitated with EZH2 and H3K27me3 antibodies was measured using the ChIP assay and RT-qPCR in normal chondrocytes and IL-1 β -treated chondrocytes (Fig. 2D, E).

According to the results, a greater amount of the miR-138 promoter was present in the immune complexes from the IL-1 β -treated chondrocytes than in normal chondrocytes ($p < 0.05$). Finally, the amount of the miR-138 promoter in the immune complexes was observed again using the ChIP assay and RT-qPCR, which showed a decrease in the amount of the miR-138 promoter in the immune complexes following EZH2 knockdown ($p > 0.05$, Fig. 2F, G). Next, we treated cells with IL-1 β alone or in combination with 3-deazaneplanocin A and performed a Western blot analysis to determine the levels of EZH2. Decreased EZH2 levels were observed in cells treated with IL-1 β and 3-deazaneplanocin A (Fig. 2H). Additionally, the ChIP-qPCR results revealed a much lower level of the miR-138 promoter in the immune complexes from cells treated with both IL-1 β and 3-deazaneplanocin A than in cells treated with IL-1 β alone (Fig. 2I, J). Taken together, EZH2 indeed inhibited miR-138 expression by increasing histone methylation at its promoter.

SDC1 was a target gene of miR-138

Furthermore, an analysis of DEGs was performed using the OA-related expression dataset GSE82107, and 85 DEGs were identified, including 45 upregulated and 39 downregulated genes (Fig. 3A). Then, the online STRING database was used to conduct a PPI analysis of these DEGs, and the Cytoscape software was employed to visualize the PPI results (Fig. 3B) with a degree ≥ 22 set as the threshold. Finally, 19 DEGs with prominent interactions were obtained. Subsequently, the p values of these 19 genes were compared in the GSE82107 dataset, after which the SDC1 gene with the smallest p value was obtained. SDC1 was subsequently selected as the cytokine that potentially represents a key regulator of OA. The upstream miRNA regulating SDC1 was predicted using the miRanda and the Starbase databases (Fig. 3C), and miR-138 was identified as the most probable miRNA targeting SDC1, as suggested by the existence of a binding site for miR-138 in the SDC1 mRNA predicted by the RNA22 bioinformatics website (Fig. 3D).

SDC1 expression patterns were detected in OA cartilage tissues and OA cell models using RT-qPCR and Western blot analyses to further verify these predictions (Fig. 3E, F). Higher SDC1 expression was observed in both OA cartilage tissues and OA cell models than in their relevant NC samples ($p < 0.05$). Moreover, a dual-luciferase reporter gene assay (Fig. 3G) revealed decreased luciferase activity in cells co-transfected with the WT-SDC1-3'UTR and miR-138 mimic compared to cells co-transfected with the WT-SDC1-3'UTR and NC mimic ($p < 0.05$). However, noticeable changes in luciferase activity were not detected in cells co-transfected with the MUT-SDC1-3'UTR and miR-138

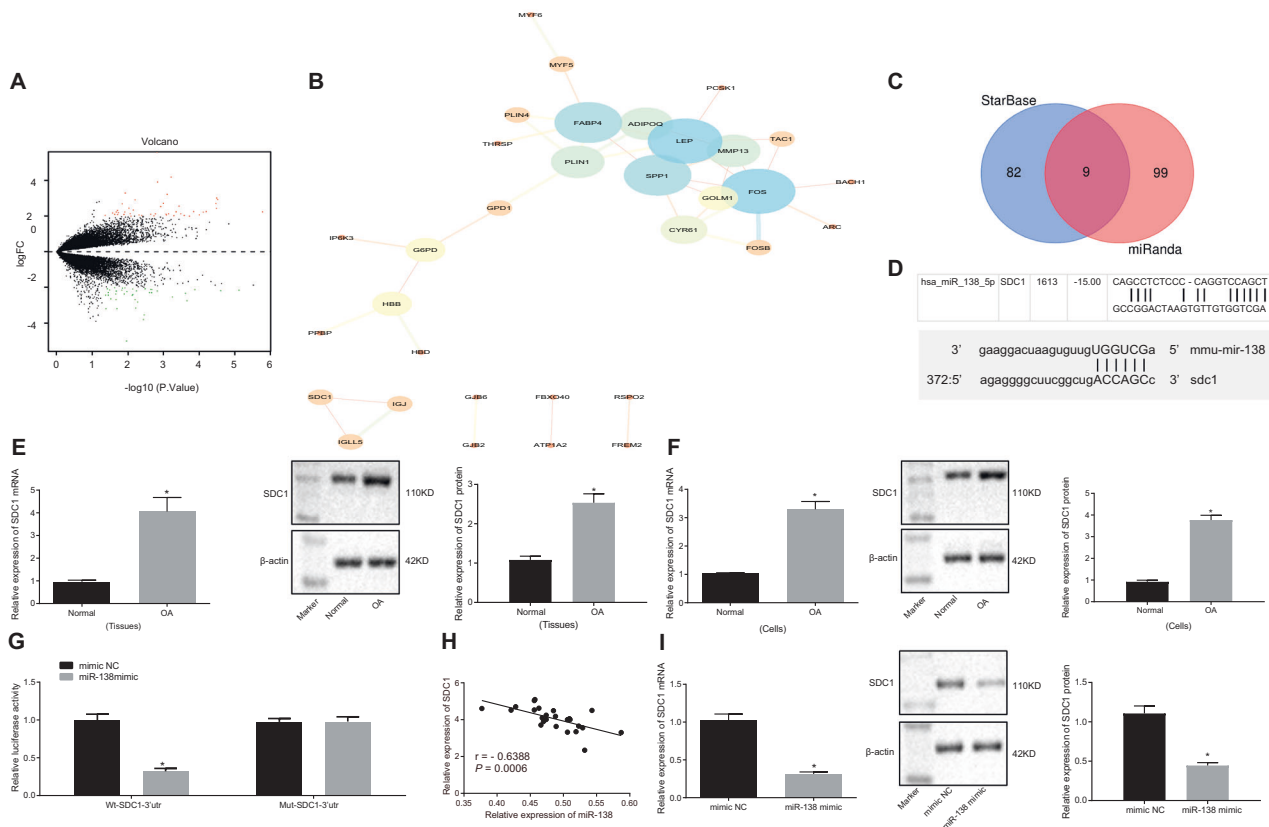


Fig. 3 miR-138 targeted SDC1 and negatively regulated its expression. **A** A volcano plot depicting the OA-related DEGs. The X-axis indicates differential log₁₀ *p* values and the Y axis represents the log fold change; each point indicates a gene. Red points indicate upregulated DEGs and green points indicate downregulated DEGs in samples from patients with OA. **B** PPI network of DEGs; a larger circle and deeper color indicate a closer PPI. **C** Regulatory miRNAs of DEGs predicted by the miRanda and Starbase databases; the number indicates the number of miRNAs. **D** Binding sites for miR-138 in the SDC1 mRNA predicted by the RNA22 website. **E**, SDC1 expression in OA cartilage tissues, as detected using RT-qPCR and western

blotting. **p* < 0.05 compared with healthy cartilage tissues (*n* = 25). **F** SDC1 expression in OA cell models, as detected using RT-qPCR and western blot analysis. **p* < 0.05 compared with normal chondrocytes. **G** The targeting relationship between miR-138 and SDC1 was verified by a dual-luciferase reporter gene assay in OA cell models. **p* < 0.05 compared with the NC mimic. **H** Correlation between miR-138 and SDC1 expression in OA cartilage tissues (*n* = 25), as determined by calculating Pearson's correlation coefficient. **I** SDC1 mRNA and protein expression in OA cell models overexpressing miR-138, as detected using RT-qPCR and western blot analysis. **p* < 0.05 compared with the NC mimic. *n* = 3.

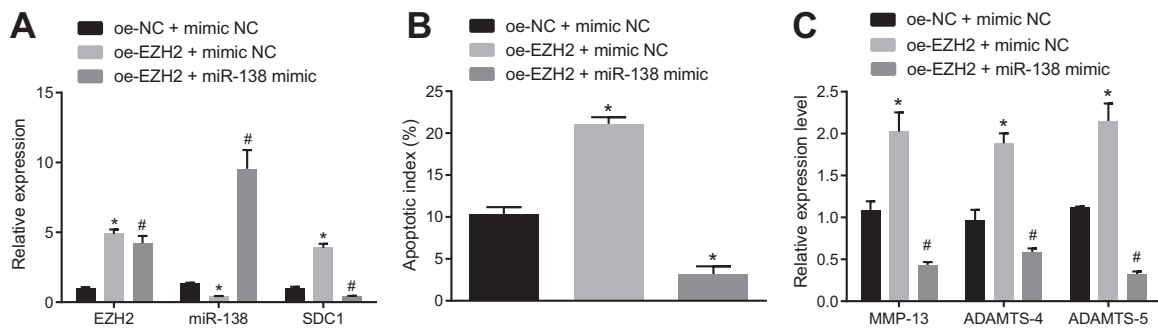


Fig. 4 The regulatory mechanism underlying the effect of the EZH2/miR-138/SDC1 axis on cartilage catabolism factors in OA cell models. **A** Expression of EZH2, miR-138 and SDC1 in OA cell models detected using RT-qPCR. **p* < 0.05 compared with OA cell models overexpressing NC and NC mimic. **B** Apoptosis in OA cell models was determined using flow cytometry. **p* < 0.05 compared with OA cell models overexpressing NC and NC mimic. #*p* < 0.05

compared with OA cell models overexpressing EZH2 and NC mimic. **C** RT-qPCR analysis of the expression of cartilage catabolism factors (MMP-13, ADAMTS-4, and ADAMTS-5) expression patterns in OA cell models. **p* < 0.05 compared with OA cell models overexpressing NC and NC mimic. #*p* < 0.05 compared with OA cell models overexpressing EZH2 and NC mimic.

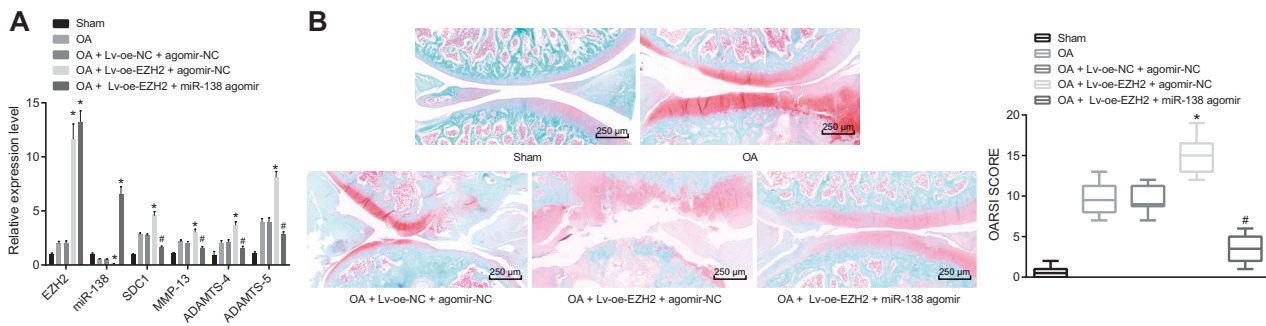


Fig. 5 The regulatory mechanism of the EZH2/miR-138/SDC1 in OA in vivo. **A** RT-qPCR analysis of EZH2, miR-138, SDC1, MMP-13, ADAMTS-4, and ADAMTS-5 expression in mouse cartilage tissues. **B** Paraffin sections of mouse cartilage tissues stained with safranin O and evaluated using the OARSI scoring system ($\times 40$). * $p < 0.05$ compared with cartilage tissues from OA mice treated with a lentivirus overexpressing NC and agomir NC. # $p < 0.05$ compared with cartilage tissues from OA mice treated with a lentivirus overexpressing EZH2 and agomir NC.

mimic ($p > 0.05$). Additionally, Pearson's correlation analysis revealed that miR-138 expression was negatively correlated with SDC1 expression in human OA cartilage tissues (Fig. 3H). Finally, the OA cell model was transfected with the miR-138 mimic and its NC (Fig. 3I), and SDC1 expression was remarkably decreased in the OA cell model transfected with miR-138 mimic compared to cells transfected with the NC mimic ($p < 0.05$). Based on these findings, SDC1 was a target gene of miR-138.

EZH2 inhibited miR-138 expression and upregulated SDC1 to promote the expression of biomarkers of cartilage catabolism in the OA cell model

With the aim of elucidating the mechanism by which the EZH2/miR-138/SDC1 axis influenced OA, cell models were transfected with the EZH2 overexpression plasmid, miR-138 mimic or their relevant NCs alone or in combination. Then, RT-qPCR was applied to detect the expression patterns of EZH2, miR-138, and SDC1 in OA cell models with various treatments (Fig. 4A). OA cell models overexpressing EZH2 and the NC mimic exhibited significantly increased EZH2 and SDC1 expression, while miR-138 expression was decreased compared to the relevant NC treatment. However, the OA cell model overexpressing EZH2 and the miR-138 mimic showed no changes in EZH2 expression, elevated miR-138 expression and decreased SDC1 expression compared with the oe-EZH2 treatment alone (all $p < 0.05$).

Additionally, cell apoptosis was detected in transfected OA cell models using flow cytometry (Fig. 4B). Apoptosis was increased in cells with EZH2 overexpression and the NC mimic but reduced in cells overexpressing EZH2 and the miR-138 mimic compared with their relevant NCs (all $p < 0.05$). Moreover, RT-qPCR (Fig. 4C) indicated significantly increased expression of MMP-13, ADAMTS-4, and ADAMTS-5 in cells overexpressing EZH2 and the NC

0.05 compared with cartilage tissues from OA mice treated with a lentivirus overexpressing NC and agomir NC. # $p < 0.05$ compared with cartilage tissues from OA mice treated with a lentivirus overexpressing EZH2 and agomir NC.

mimic, but the expression of these mRNAs was significantly downregulated in cells overexpressing EZH2 and the miR-138 mimic compared to the NCs (all $p < 0.05$). Therefore, EZH2 induced the expression of cartilage catabolism-related factors by regulating miR-138/SDC1 signaling.

EZH2 accelerated cartilage degeneration through the methylation of histones at the miR-138 promoter in vivo

Cartilage degeneration is a fundamental pathological feature of OA, and thus the progression of cartilage degeneration in mice was analyzed after the modulation of the EZH2/miR-138/SDC1 axis. Mice were assigned to the sham group, the OA group, the OA + Lv-oe-NC + agomir-NC group, the OA + Lv-oe-EZH2 + agomir-NC group, and the OA + Lv-oe-EZH2 + miR-138 agomir group. Subsequently, the expression of EZH2, miR-138, SDC1, MMP-13, ADAMTS-4, and ADAMTS-5 was detected in the cartilage tissues from mouse knee joints using RT-qPCR. The expression of EZH2, SDC1, MMP-13, ADAMTS-4, and ADAMTS-5 was significantly increased and miR-138 expression was decreased in the OA + Lv-oe-EZH2 + agomir-NC group. On the other hand, miR-138 expression was increased and SDC1 expression was reduced, but no changes in EZH2 expression were observed in the OA + Lv-oe-EZH2 + miR-138 agomir group compared to the OA + Lv-oe-EZH2 + agomir-NC group (all $p < 0.05$) (Fig. 5A).

Thereafter, paraffinized cartilage tissue sections from mouse knee joints were prepared, stained with safranin O and subjected to histological scoring according to the standard provided by OARSI. Mice in the OA + Lv-oe-EZH2 + agomir-NC group showed thinner cartilage tissues, accelerated cartilage destruction, proteoglycan loss, a relatively increased loss of bone trabecula connection

density and an increased degree of bone trabecular directional distribution of cortical bone, accompanied by a higher score evaluated according to the OARSI criteria. However, the cartilage tissues were thicker in the mice from the OA + Lv-oe-EZH2 + miR-138 agomir group, as cartilage destruction was reduced, proteoglycan loss was decreased and the loss of bone trabecula connection density was inhibited to result in a lower OARSI score (all $p < 0.05$) (Fig. 5B). Based on these findings, EZH2 promoted cartilage degeneration in OA mice by regulating miR-138/SDC1 signaling.

Discussion

Epigenetic regulation is achieved through various mechanisms, such as genomic DNA methylation and histone modifications [22]. However, its role in OA remains to be elucidated. The role of miRNAs in the progression of OA is well established, and miR-21-5p [23] and miR-186 [24] have been identified as prospective therapeutic targets for OA. However, to date, the association between these target miRNAs and their epigenetic regulation in OA, which might be a key mechanism contributing to their functions, has not been investigated. Therefore, in the current study, both OA cell and OA mouse models were established. Our data not only described the methylation of histones at the miR-138 promoter and its effect on OA but also revealed the regulatory mechanism underlying the effect of EZH2 on miR-138 methylation in OA. Moreover, the pro-inflammatory factor IL-1 β is well-regarded as a main pathological factor in OA [20]. Thus, we attempted to establish cell models of OA induced by IL-1 β using the methods described in previous studies, in which chondrocytes were treated with IL-1 β for 24 h to establish the OA cell model [25, 13]. Hence, EZH2 may represent a novel biomarker of articular cartilage degeneration in individuals with OA.

Notably, EZH2 is a histone methyltransferase that is reported to be associated with several types of skeletal tissue dysfunction [26]. In addition, the methyltransferase EZH2 functions in regulating the expression of the long non-coding RNA MEG3 and is also implicated in chondrogenic differentiation, suggesting that EZH2 may have a critical role in regulating OA [27]. However, another study documented increased levels of EZH2 in subjects with OA, changes that were suppressed by the administration of 3-deazaneplanocin A [28]. OA and healthy cartilage tissues, as well as OA and normal chondrocytes were used in the present study; our data further verified that EZH2 was expressed at high levels in OA samples. Subsequently, we investigated the mechanism by which EZH2 affected OA. EZH2 silencing significantly reduced the expression of

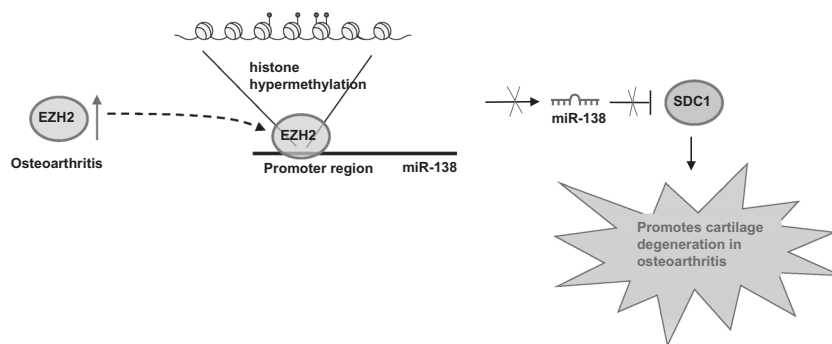
cartilage catabolism factors, including MMP-13, ADAMTS-4, and ADAMTS-5. Moreover, reduced cell apoptosis and MMP-13, ADAMTS-4, and ADAMTS-5 levels were also observed upon silencing of EZH2. Consistent with the results of our study, MMP-13, ADAMTS-4, and ADAMTS-5 expression are closely related to anabolic activity and OA [29]. Moreover, the changes in the expression of these matrix-degrading enzymes (MMP-13, ADAMTS-4, and ADAMTS-5) suggest a novel trend in cell apoptosis [30]. Therefore, EZH2 potentially accelerated the progression of OA, while the knockdown of EZH2 effectively ameliorated OA.

Based on the findings described above, we speculated that a better understanding of the downstream mechanism of EZH2 in OA would be very important. Interestingly, previous studies have reported the aberrant expression of miR-138 and its role in OA, illustrating that miR-138 was expressed at low levels in OA tissues and suppressed OA [21]. Notably, the EZH2 is also known to be associated with the regulation of miRNAs involved in chondrogenic differentiation in individuals with renal cell cancer [31]. Additionally, miR-138 functions as a tumor suppressor and negatively regulate EZH2 in renal cell cancer [32]. In the current study, we discovered that miR-138 was negatively correlated with EZH2 expression in OA samples.

Furthermore, in our study, ChIP-qPCR was conducted in a series of OA cell models to measure the quantity of the miR-138 promoter in the immune complexes generated using EZH2 and H3K27me3 antibodies. EZH2 methylated histones at the miR-138 promoter and then subsequently inhibited miR-138 expression. Notably, the findings from the present study were distinguished from previously reported studies that have rarely discussed the relationship between EZH2 and methylated miR-138.

The discovery of the relationship between EZH2 and miR-138 allowed us to determine the role of miR-138 in OA. Our results obtained from the STRING online database and Cytoscape software illustrated that SDC1 was the DEG with the lowest p value in the GSE82107 microarray. Recent studies have highlighted the involvement of SDC4 in the altered expression of cartilage catabolism factors (MMP-13, ADAMTS-4, and ADAMTS-5), whereas upregulated SDC4 has been shown to exacerbate the dysfunction of articular cartilage [33]. Consistent with these reports, miR-138 targeted SDC1 in the present study. Notably, miR-138 promotes cartilage degeneration in human chondrocytes via FOXC1 [34]. SDC1 expression has been reported to be upregulated in the early stage of articular cartilage degeneration [35]. However, SDC1 expression is suppressed by miR-494 to modulate the epithelial-mesenchymal transition, migration, and invasion in pancreatic cancer [36].

Fig. 6 The mechanism of EZH2/miR-138/SDC1 axis in OA. EZH2 downregulated miR-138 expression and then increased SDC1 expression through histone methylation at the miR-138 promoter during OA development.



As shown in the present study, EZH2 downregulated the expression of miR-138 and increased SDC1 expression through the methylation of histones at the miR-138 promoter during OA development (Fig. 6). Moreover, the EZH2-mediated regulatory mechanism also facilitated cartilage degeneration in OA mouse models. Collectively, the aforementioned results confirmed the requirement for EZH2 in the process of cartilage degeneration in OA. Nonetheless, in-depth studies are required to highlight the regulatory effects of SDC1 on both cartilage degeneration and OA and its associated epigenetic mechanisms underlying OA. Moreover, our current research is still in the theoretical stage with no clinical trials involved. However, in further studies, we will employ the DZNep mouse model to verify the findings of the present study and potentially develop effective therapies to treat OA.

Acknowledgements We acknowledge and appreciate our colleagues for their valuable assistance and comments on this paper.

Funding This study was supported by grants from the Scientific Research Project of the Shanghai Municipal Health and Planning Committee (20204Y0365), and Shanghai Committee of Science and Technology (17ZR1416600 and 19ZR1429200).

Compliance with ethical standards

Conflict of interest The authors declare that they have no conflict of interest.

Ethical approval The collection of human tissues samples was approved by the Ethics Committee of Shanghai Ninth People's Hospital, Shanghai Jiao Tong University School of Medicine, and sample collection was performed in strict accordance with the approved guidelines. All participants signed informed consent documents. Animal experiments were conducted according to the *Guide for the Care and Use of Laboratory Animals* published by the National Institutes of Health and approved by the Animal Care and Use Committees of Shanghai Ninth People's Hospital, Shanghai Jiao Tong University School of Medicine. We attempted to minimize the suffering of the included animals to the greatest extent possible.

Publisher's note Springer Nature remains neutral with regard to jurisdictional claims in published maps and institutional affiliations.

References

- Melrose J. The importance of the knee joint meniscal fibrocartilages as stabilizing weight bearing structures providing global protection to human knee-joint tissues. *Cells*. 2019;8:324.
- Sudirman S, Chang HW, Chen CK, Kong ZL. A dietary polysaccharide from *Eucheuma cottonii* downregulates proinflammatory cytokines and ameliorates osteoarthritis-associated cartilage degradation in obese rats. *Food Funct*. 2019;10:5697–706.
- Nomura M, Sakitani N, Iwasawa H, Kohara Y, Takano S, Wakimoto Y, et al. Thinning of articular cartilage after joint unloading or immobilization. An experimental investigation of the pathogenesis in mice. *Osteoarthritis Cartilage*. 2017;25:727–36.
- Carballo CB, Nakagawa Y, Sekiya I, Rodeo SA. Basic science of articular cartilage. *Clin Sports Med*. 2017;36:413–25.
- Wang X, Tang D, Shen P, Xu H, Qiu H, Wu T, et al. Analysis of DNA methylation in chondrocytes in rats with knee osteoarthritis. *BMC Musculoskelet Disord*. 2017;18:377.
- Frapporti A, Miro Pina C, Arnaiz O, Holoch D, Kawaguchi T, Humbert A, et al. The Polycomb protein Ezh1 mediates H3K9 and H3K27 methylation to repress transposable elements in *Paramecium*. *Nat Commun*. 2019;10:2710.
- Chen L, Wu Y, Wu Y, Wang Y, Sun L, Li F. The inhibition of EZH2 ameliorates osteoarthritis development through the Wnt/beta-catenin pathway. *Sci Rep*. 2016;6:29176.
- Lian WS, Ko JY, Wu RW, Sun YC, Chen YS, Wu SL, et al. MicroRNA-128a represses chondrocyte autophagy and exacerbates knee osteoarthritis by disrupting Atg12. *Cell Death Dis*. 2018;9:919.
- Xu W, Gao P, Zhang Y, Piao L, Dong D. microRNA-138 induces cell survival and reduces WNT/beta-catenin signaling of osteoarthritis chondrocytes through NEK2. *IUBMB Life*. 2019;71:1355–66.
- Rastgoo N, Pourabdollah M, Abdi J, Reece D, Chang H. Dysregulation of EZH2/miR-138 axis contributes to drug resistance in multiple myeloma by downregulating RBPMS. *Leukemia*. 2018;32:2471–82.
- Kong Y, Wang W, Zhang C, Wu Y, Liu Y, Zhou X. Cannabinoid WIN55,2122 mesylate inhibits ADAMTS4 activity in human osteoarthritic articular chondrocytes by inhibiting expression of syndecan1. *Mol Med Rep*. 2016;13:4569–76.
- Wang M, Liu C, Zhang Y, Hao Y, Zhang X, Zhang YM. Protein interaction and microRNA network analysis in osteoarthritis meniscal cells. *Genet Mol Res*. 2013;12:738–46.
- Lou Y, Wang C, Zheng W, Tang Q, Chen Y, Zhang X, et al. Salvianolic acid B inhibits IL-1beta-induced inflammatory cytokine production in human osteoarthritis chondrocytes and has a protective effect in a mouse osteoarthritis model. *Int Immunopharmacol*. 2017;46:31–7.

14. Gu XD, Wei L, Li PC, Che XD, Zhao RP, Han PF, et al. Adenovirus-mediated transduction with Histone Deacetylase 4 ameliorates disease progression in an osteoarthritis rat model. *Int Immunopharmacol.* 2019;75:105752.
15. Wang Q, Zheng J, Zou JX, Xu J, Han F, Xiang S, et al. S-adenosylhomocysteine (AdoHcy)-dependent methyltransferase inhibitor DZNep overcomes breast cancer tamoxifen resistance via induction of NSD2 degradation and suppression of NSD2-driven redox homeostasis. *Chem Biol Interact.* 2020; 317:108965.
16. Xie Y, Wang M, Shao Y, Deng X, Chen Y. Long non-coding RNA KCNQ1OT1 contributes to antiepileptic drug resistance through the miR-138-5p/ABCB1 axis in vitro. *Front Neurosci.* 2019;13:1358.
17. Yu C, Ding B, Zhang X, Deng X, Deng K, Cheng Z, et al. Targeted iron nanoparticles with platinum-(IV) prodrugs and anti-EZH2 siRNA show great synergy in combating drug resistance in vitro and in vivo. *Biomaterials.* 2018;155:112–23.
18. Jian MY, Koizumi T, Tsushima K, Yokoyama T, Kubo K, Baba A. Exogenous surfactant instillation attenuates inflammatory response to acid-induced lung injury in rat. *Pulm Pharmacol Ther.* 2010;23:43–7.
19. Wang H, Zhang H, Sun Q, Wang Y, Yang J, Yang J, et al. Intra-articular delivery of antago-miR-483-5p inhibits osteoarthritis by modulating matrilin 3 and tissue inhibitor of metalloproteinase 2. *Mol Ther.* 2017;25:715–27.
20. Rai MF, Rachakonda PS, Manning K, Vorwerk B, Brunnberg L, Kohn B, et al. Quantification of cytokines and inflammatory mediators in a three-dimensional model of inflammatory arthritis. *Cytokine.* 2008;42:8–17.
21. Wei ZJ, Liu J, Qin J. miR-138 suppressed the progression of osteoarthritis mainly through targeting p65. *Eur Rev Med Pharmacol Sci.* 2017;21:2177–84.
22. Simon TC, Jeffries MA. The epigenomic landscape in osteoarthritis. *Curr Rheumatol Rep.* 2017;19:30.
23. Wang XB, Zhao FC, Yi LH, Tang JL, Zhu ZY, Pang Y, et al. MicroRNA-21-5p as a novel therapeutic target for osteoarthritis. *Rheumatology.* 2019. <https://doi.org/10.1093/rheumatology/kez102>.
24. Lin Z, Tian XY, Huang XX, He LL, Xu F. microRNA-186 inhibition of PI3K-AKT pathway via SPP1 inhibits chondrocyte apoptosis in mice with osteoarthritis. *J Cell Physiol.* 2019;234:6042–53.
25. Pan T, Wu D, Cai N, Chen R, Shi X, Li B, et al. Alpha-Mangostin protects rat articular chondrocytes against IL-1beta-induced inflammation and slows the progression of osteoarthritis in a rat model. *Int Immunopharmacol.* 2017;52:34–43.
26. van Wijnen AJ, Westendorf JJ. Epigenetics as a new frontier in orthopedic regenerative medicine and oncology. *J Orthop Res.* 2019;37:1465–74.
27. You D, Yang C, Huang J, Gong H, Yan M, Ni J. Long non-coding RNA MEG3 inhibits chondrogenic differentiation of synovium-derived mesenchymal stem cells by epigenetically inhibiting TRIB2 via methyltransferase EZH2. *Cell Signal.* 2019;63:109379.
28. Aury-Landas J, Bazille C, Allas L, Bouhout S, Chesneau C, Leclercq S, et al. Anti-inflammatory and chondroprotective effects of the S-adenosylhomocysteine hydrolase inhibitor 3-Deazaneplanocin A, in human articular chondrocytes. *Sci Rep.* 2017;7:6483.
29. Blasioli DJ, Kaplan DL. The roles of catabolic factors in the development of osteoarthritis. *Tissue Eng Part B Rev.* 2014;20:355–63.
30. Latourte A, Cherifi C, Maillet J, Ea HK, Bouaziz W, Funck-Brentano T, et al. Systemic inhibition of IL-6/Stat3 signalling protects against experimental osteoarthritis. *Ann Rheum Dis.* 2017;76:748–55.
31. Wang P, Li Y, Meng T, Zhang J, Wei Y, Meng Z, et al. KDM6A promotes chondrogenic differentiation of periodontal ligament stem cells by demethylation of SOX9. *Cell Prolif.* 2018;51: e12413.
32. Liang J, Zhang Y, Jiang G, Liu Z, Xiang W, Chen X, et al. MiR-138 induces renal carcinoma cell senescence by targeting EZH2 and is downregulated in human clear cell renal cell carcinoma. *Oncol Res.* 2013;21:83–91.
33. Binch ALA, Shapiro IM, Risbud MV. Syndecan-4 in intervertebral disc and cartilage: Saint or synner? *Matrix Biol.* 2016;52-54:355–62.
34. Yuan Y, Zhang GQ, Chai W, Ni M, Xu C, Chen JY. Silencing of microRNA-138-5p promotes IL-1beta-induced cartilage degradation in human chondrocytes by targeting FOXC1: miR-138 promotes cartilage degradation. *Bone Jt Res.* 2016;5:523–30.
35. Salminen-Mankonen H, Saamanen AM, Jalkanen M, Vuorio E, Pirila L. Syndecan-1 expression is upregulated in degenerating articular cartilage in a transgenic mouse model for osteoarthritis. *Scand J Rheumatol.* 2005;34:469–74.
36. Yang Y, Tao X, Li CB, Wang CM. MicroRNA-494 acts as a tumor suppressor in pancreatic cancer, inhibiting epithelial-mesenchymal transition, migration and invasion by binding to SDC1. *Int J Oncol.* 2018;53:1204–14.